Inorganic Chemistry

ARTICLE

pubs.acs.org/IC

Hydration Structure of the Ti(III) Cation as Revealed by Pulse EPR and DFT Studies: New Insights into a Textbook Case

Sara Maurelli, Stefano Livraghi, Mario Chiesa,* and Elio Giamello

Dipartimento di Chimica IFM, Università di Torino and NIS, Nanostructured Interfaces and Surfaces Centre of Excellence, Via P. Giuria 7, I-10125 Torino, Italy

Sabine Van Doorslaer

University of Antwerp, Department of Physics, Universiteitsplein 1, B-2610 Wilrijk-Antwerp, Belgium

Cristiana Di Valentin and Gianfranco Pacchioni

Dipartimento di Scienza dei Materiali, Università di Milano-Bicocca, Via R. Cozzi, 53-20125, Milano, Italy

Supporting Information

ABSTRACT: The ^{17}O and ^{1}H hyperfine interactions of water ligands in the Ti(III) aquo complex in a frozen solution were determined using Hyperfine Sublevel Correlation (HYSCORE) and Pulse Electron Nuclear Double Resonance (ENDOR) spectroscopies at 9.5 GHz. The isotropic hyperfine interaction (hfi) constant of the water ligand ^{17}O was found to be about 7.5 MHz. ^{1}H Single Matched Resonance Transfer (SMART) HYSCORE spectra allowed resolution of the hfi interactions of the two inequivalent water ligand protons and the relative orientations of their hfi tensors. The magnetic and geometrical parameters extracted from the experiments were compared with the results of DFT computations for different geometrical arrangements of the water ligands around the cation. The theoretical observable properties (**g** tensor ^{1}H and ^{17}O hfi tensors and their orientations) of the $[Ti(H_2O)_6]^{3+}$ complex are in quantitative agreement with the experiments for two slightly different geometrical arrangements associated with D_{3d} and C_i symmetries.

INTRODUCTION

Ionic hydration, i.e., the interaction of metal ions with water, has been an attractive subject to chemists ever since the time of Arrhenius for both fundamental and applied reasons.[1,2] A paradigmatic case is that of the esahydrated complex $[Ti(H_2O)_6]^{3+}$.

Ti^{3+} is a prototypical paramagnetic metal ion, which is of importance in both homogeneous and heterogeneous catalysis.[3] Due to the paramagnetic nature of this ion, electron paramagnetic resonance (EPR) has been widely employed in its characterization and has led to singular progress in the understanding of its electronic and geometrical features in different environments.[4]

$[Ti(H_2O)_6]^{3+}$ is usually taken as a textbook example to illustrate the effect of ligand field theory on splitting degenerate d orbitals.[5] However, despite its seeming simplicity, the details of the hydration structure and the nature of ground and excited electronic states of this esaquo complex are often oversimplified and misinterpreted.

EPR, electron nuclear double resonance (ENDOR), and electron spin−echo (ESE) techniques have been employed in the past to characterize the solvation structure of Ti^{3+} ions in glassy water, suggesting that the hydrated ion has D_{3d} symmetry with the unpaired electron dwelling in the d_{z^2} orbital.[6] The electronic transition in the visible range appearing at around 500 nm with a shoulder at 570 nm was thus assigned with the help of *ab initio* molecular orbital calculations to $^{2}A_{1g} \rightarrow {}^{2}E'_{g}$ transitions, whereby the degeneracy of the $^{2}E'_{g}$ excited states is removed by a dynamic Jahn−Teller effect.[7]

The above conclusions were obtained on the basis of the fitting of electron spin−echo envelope modulation (ESEEM) patterns and quantum-chemical calculations; however, no detailed determination of the proton hyperfine coupling constants of the water molecules coordinated to Ti(III) ions is available. Moreover, to the best of our knowledge, no data relative to the spin density repartition over the coordinating oxygens are present in the literature, which are of crucial importance in evaluating the nature of the chemical bond and the geometrical arrangements of water ligands.

^{17}O is an important probe used to investigate the essential chemical and geometrical features in metal−oxygen coordination and bonding, which is a recurrent theme in diverse areas from biology to catalysis and material science. In most cases, the hyperfine and nuclear quadrupole couplings of the surrounding magnetic nuclei are not resolved in the conventional field swept EPR spectrum. A large variety of techniques exists, however, that allow detection of these interactions, such as ESEEM, ENDOR, and ELDOR (electron−electron double resonance) detected NMR.[8] As an example, the ^{17}O hyperfine interaction in esaquo

Received: October 29, 2010
Published: February 11, 2011

VO^{2+}, Mn^{2+}, and Gd^{3+} hydrated ions has been determined by means of high field ENDOR,[9,10] while HYSCORE experiments have been employed to determine the ^{17}O hyperfine interaction of water molecules coordinated to molybdenum enzymes,[11] the oxygen-evolving complex of photosystem II,[12] or the metal oxygen interaction at an oxide surface.[13]

In the present work, we revisit the water coordination chemistry of Ti^{3+} ions by using ^{17}O-enriched water, HYSCORE spectroscopy, and advanced quantum-chemical calculations to compute, from first principles, both the **g** tensor and the hyperfine coupling constants. The ^{1}H hyperfine and ^{17}O hyperfine and quadrupole interactions are resolved for the first time.

The chemistry of Ti^{3+} is very diverse and involves important chemical and photochemical reactions which often occur in aqueous environments; however, there is a large lack in reference EPR data on Ti^{3+} complexes to which to compare. We believe that this in-depth characterization of the $Ti(H_2O)_6^{3+}$ complex will be of importance in the general problem of addressing the nature of Ti^{3+} species in different and complex materials of practical importance.

EXPERIMENTAL AND COMPUTATIONAL METHODS

Sample Preparation. The $[Ti(H_2O)_6]^{3+}$ complex was prepared contacting a solution (~6 mM) of $TiCl_4$ (99.0% Sigma Aldrich) in HCl (5M) with metallic Zn until the liquid changed color from colorless to pale pink. Isotopically (^{17}O) labeled Ti complex was obtained using $H_2{}^{17}O$ (isotec 40%) in the preparation. During the synthesis, the isotopically enriched water was further diluted, reaching a nominal concentration in ^{17}O of about 30−35%. Under these circumstances, only ~50% of the complexes will have one or more ^{17}O-labeled water molecules in its coordination sphere, whereby ~25% of the complexes have only one ^{17}O nucleus and ~12.6% have two ^{17}O nuclei. This is however sufficient for EPR/ENDOR spectroscopy means.

Spectroscopic Measurements. X-band CW EPR spectra were detected at 77 K on a Bruker EMX spectrometer (microwave frequency, 9.75 GHz) equipped with a cylindrical cavity. A microwave power of 1 mW, a modulation amplitude of 0.1 mT, and a modulation frequency of 100 kHz was used. Pulse EPR experiments were performed on an ELEXYS 580 Bruker spectrometer (at a microwave frequency of 9.76 GHz) equipped with a liquid-helium cryostat from Oxford Inc. All experiments were performed at 10 K unless elsewhere stated. The magnetic field was measured by means of a Bruker ER035 M NMR gaussmeter.

Electron-spin−echo (ESE) detected EPR experiments were carried out with the pulse sequence: $\pi/2-\tau-\pi-\tau-$echo, with microwave pulse lengths $t_{\pi/2}$ = 16 ns and t_π = 32 ns and a τ value of 200 ns.

Davies-ENDOR spectra shown in Figure 5 were measured with the mw pulse sequence $\pi-T-\pi/2-\tau-\pi-\tau-$echo, with mw pulses of length $t_{\pi/2}$ = 16 ns and t_π = 32 ns, and τ = 220 ns. A radio frequency pulse of length 12 μs and variable frequency ν_{ENDOR} were applied during time T. These settings were found to be optimal to detect the ^{17}O contributions. Other settings were used when focusing only on the ^{1}H contributions, as shown in the Supporting Information. The Davies-ENDOR spectra were simulated using the Easyspin program.[14]

Hyperfine Sublevel Correlation (HYSCORE) experiments[15] were carried out with the pulse sequence $\pi/2-\tau-\pi/2-t_1-\pi-t_2-\pi/2-\tau-$echo with a microwave pulse length $t_{\pi/2}$ = 16 ns and t_π = 16 ns. The time intervals t_1 and t_2 were varied in steps of 8 or 16 ns starting from 96 to 3296 ns. A four-step phase cycle was used for eliminating unwanted echoes. In order to avoid blind spot effects, different τ values were chosen, which are specified in the figure captions. The corresponding HYSCORE spectra were added after Fourier transformation.

The *SMART HYSCORE*[16,17] sequence is $p_M-t_1-\pi-t_2-p_M-\tau-\pi-\tau-$echo ($p_M$ = high-turning angle (HTA) matched pulse). The matching-pulse field strength, ν_1, was taken to be 15.625 MHz. The length of the matching pulse was optimized using a matched three-pulse ESEEM experiment.[17] The optimal value was found to be 40 ns. The length of the π pulses was taken to be 16 ns. A four-step phase cycle was used to eliminate unwanted echoes.

The time traces of the HYSCORE spectra were baseline corrected with a third-order polynomial, apodized with a Hamming window and zero filled. After two-dimensional Fourier transformation, the absolute value spectra were calculated. The spectra were added for the different τ values in order to eliminate blind-spot effects. The HYSCORE spectra were simulated using a program developed at ETH Zurich.[18]

Computational Details. The Gaussian 03 program package[19] has been used to calculate optimized geometries, electronic structure, EPR parameters (**g**, hyperfine and nuclear quadrupole tensors), and electronic transitions for the $[Ti(H_2O)_6]^{3+}$ complex. Different point symmetries have been investigated: D_{3d}, D_{2h}, and C_i. For geometry optimization, a LANL2 pseudopotential for core electrons together with the corresponding LANL2DZ basis set[20] for valence electrons was used for the Ti ion, while the O and H atoms were treated with a 6-311+G** basis set.[21] For the computation of the EPR properties and electronic transitions, larger basis sets were used: 6-311+G** for the Ti ion and EPR-II[22] for O and H atoms. Results from several density functionals have been compared, varying for the degree of exact exchange included: from 0% exact exchange of BLYP[23,24] to 13% exact exchange in B-HF(13)-LYP, to 20% exact exchange in the popular B3LYP,[24,25] to 30% exact exchange in B-HF(30)-LYP. The solvent effect (water) has also been investigated by means of the PCM[26] (polarizible continuum model) method. Electronic transitions were computed using TD-DFT[27] (time-dependent).

The hyperfine interactions of the electron spin with the nuclear spin of the ^{1}H and ^{17}O nuclei have been determined. The hyperfine spin-Hamiltonian, $H_{hfc} = \mathbf{S}\cdot\mathbf{A}\cdot\mathbf{I}$, is given in terms of the hyperfine matrix **A**, which describes the coupling of the electron with the nuclear spin. **A** can be represented as the sum of an isotropic (a_{iso}) and a dipolar part **T** (**T** is 3×3 traceless matrix). To quantify the deviations of the g values of Ti^{3+} complexes from the free electron value g_e, spin−orbit interaction must be either accounted for self-consistently or treated as a perturbation. Here, we use the spin−orbit perturbation strategy in the scheme proposed by Neese[28] and implemented in the Gaussian 03 code.

RESULTS

CW-EPR and UV−Vis Absorption Spectroscopy. Ti^{3+} ions have been generated by reducing an acidic solution of $TiCl_4$ with metallic Zn. Upon reduction, the solution develops a pale pink color. The CW-EPR and optical absorption spectra are shown in Figure 1.

The UV−vis absorption spectrum shows a characteristic absorption at about 500 nm with a shoulder at 570 nm, while the EPR powder pattern displays a pseudo-axial symmetry with $g_\parallel$ = 1.994 and $g_\perp$ = 1.896. Both spectra are in accord with previous literature reports.[6,29]

The **g** tensor for a d^1 system such as the Ti^{3+} ion is strongly dependent on the local geometry and crystal-field parameters. The experimental CW-EPR spectrum (Figure 1a) is characterized by $g_\parallel \cong g_e > g_\perp$, which for this system is usually explained by a trigonally distorted octahedral (D_{3d}) symmetry and the unpaired electron localized in a d_{z^2} orbital of the Ti^{3+} ion.[6,29−31] Similar g factors have indeed been observed for Ti(III) acetylacetonate ions substituted in the Al(III) lattice for which D_{3d} symmetry was established by crystal structure work.[32] Even though D_{3d} symmetry does account for the observed g factor splittings, it should be noted that first principle calculations suggest that lower symmetry structures (C_i point group) represent the global

dx.doi.org/10.1021/ic1021802 |*Inorg. Chem.* 2011, 50, 2385–2394

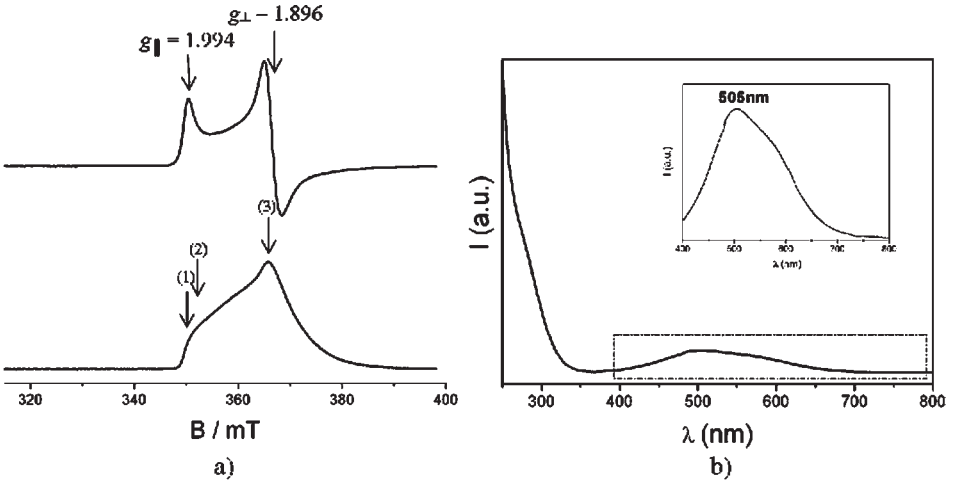

Figure 1. (a) CW-EPR (above) and ESE-detected EPR (below) spectra of hydrated Ti^{3+} in a water solution taken at T = 10 K. Numbers in brackets indicate the field positions at which HYSCORE experiments were performed. (b) Corresponding optical absorption spectrum recorded at room temperature.

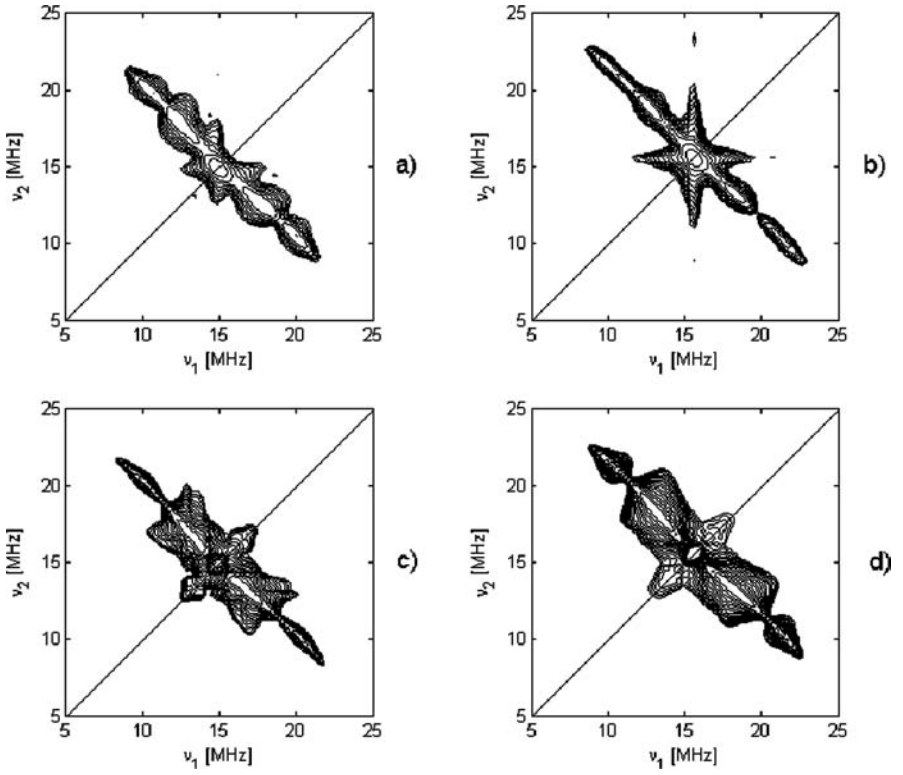

Figure 2. ^{1}H HYSCORE spectra of $Ti(H_2O)_6^{3+}$ taken at an observer position corresponding with (a) $g = g_\parallel$, (b) $g = g_\perp$, and (c and d) simulation of a and b using the parameters from Table 1. The HYSCORE spectra taken at two τ values (96 and 176 ns) are summed together after Fourier transformation.

energy minimum for the hydrated Ti(III) ion.[33,34] We shall address this aspect in the following sections. It should be noted that the CW-EPR spectrum reported in Figure 1a is characterized by a relatively large broadening and departure from ideal axial symmetry of the perpendicular spectral component. This can be explained considering strain effects induced by a plurality of hydration structures, which slightly differ one from another, together with a deviation from the ideal D_{3d} symmetry of the complex.

^{1}H HYSCORE Spectra. The hyperfine interaction of the unpaired electron with the protons of the coordinated water molecules is resolved by means of HYSCORE spectroscopy. HYSCORE is a two-dimensional experiment where correlation of nuclear frequencies in one electron spin (m_S) manifold to nuclear frequencies in the other manifold is created by means of a mixing π pulse. HYSCORE spectra taken at magnetic fields corresponding to $g = g_\parallel$ and $g = g_\perp$ are shown in Figure 2. The spectra are characterized by a pronounced ridge in the (+,+)

dx.doi.org/10.1021/ic1021802 |*Inorg. Chem.* 2011, 50, 2385–2394

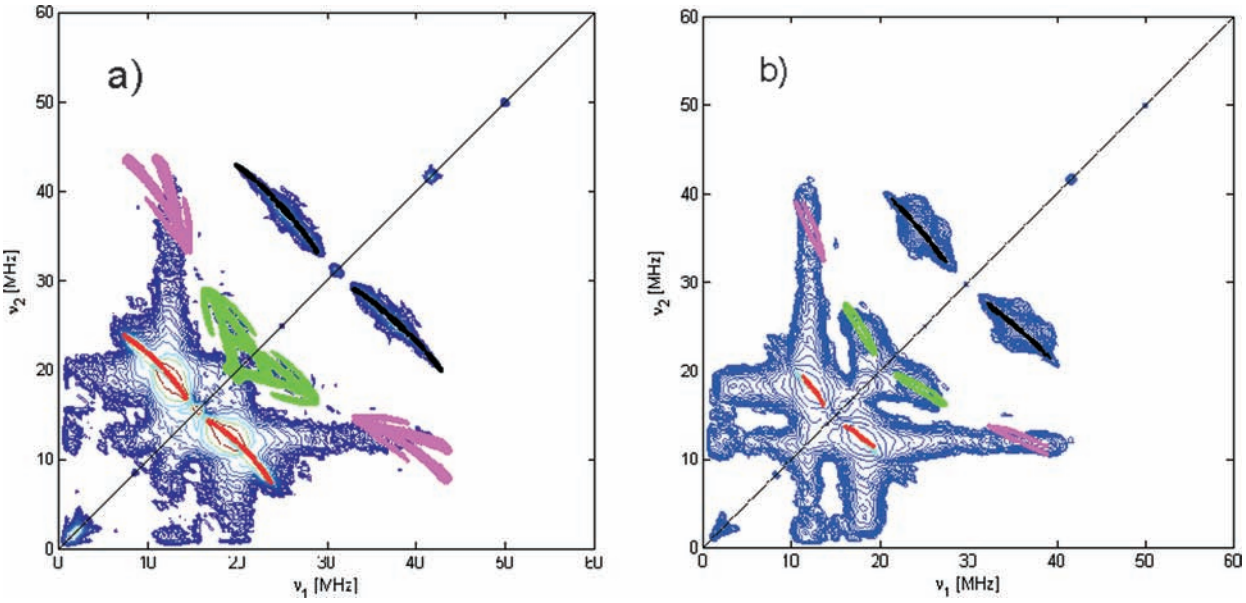

Figure 3. ^{1}H SMART HYSCORE spectra taken at an observer position corresponding to (a) $g = g_\perp$ (position 3 in Figure 1a), (b) $g = g_\parallel$ (position 1 in Figure 1a). The spectra were symmetrized to obtain a better comparison with the simulations. Furthermore, low contour limits were taken in the representation so that the reader can also evaluate the weaker cross peaks. The spectra were recorded using $\tau = 96$ ns. The simulations of the correlation ridges expected for a three-spin system $S = 1/2$, $I_a = 1/2$, and $I_b = 1/2$ assuming the HFC reported in Table 1 are superimposed on the experimental spectra. See text for color coding.

Table 1. Spin −Hamiltonian Parameters Extracted from the HYSCORE Spectra[a]

$^{H}A_\perp$	$^{H}A_\parallel$	α, β, γ	$^{O}A_{xx}$	$^{O}A_{yy}$	$^{O}A_{zz}$	α, β, γ	$\lvert e^2qQ/h\rvert$	η	α, β, γ
3.5 ± 0.2	15.5 ± 0.2	0, 70 ± 5, 0	7.0 ± 0.5	9.5 ± 0.5	6.0 ± 0.5	0, 64, 0	6.0 ± 0.5	0.5 ± 0.1	0, 31, 0
1.5 ± 0.2	11.4 ± 0.2	0, 50 ± 5, 0							

[a] All tensor values are in MHz, while Euler angles are given in degrees. The rotation of the hyperfine versus the **g** tensor is assumed, whereby β represents the rotation around the y axis and describes the orientation of the $A_\parallel$ axis with respect to $g_\parallel$ axis. The Euler angles of the ^{17}O hyperfine and quadrupole tensors are taken from the results of the DFT computations. Due to the symmetry of the system (D_{3d}), six different tensor orientations are possible (i.e., $\alpha = 0° + n60°$, where n ranges from 1 to 3 for $\beta = 64°$ and $\alpha = 0° + n30°$, $n = 1-3$, $\beta = 116°$).

quadrant, centered at about 15 MHz (the ^{1}H Larmor frequency) with a width of about 12.8 MHz at the $g_\parallel$ position and about 15.8 MHz at the $g_\perp$ position. Since the unpaired electron in the hydrated molecule is coupled to several ^{1}H nuclei, double quantum (DQ) peaks are observed in the HYSCORE spectrum centered around twice the ^{1}H Larmor frequency, which correspond to correlations between sum frequencies. In order to enhance these features, together with other combination peaks that can reveal a wealth of information concerning different hyperfine tensors and their mutual orientation, SMART HYSCORE spectra have been recorded at two observer positions (Figure 3). In these SMART HYSCORE spectra, correlation of double quantum (DQ) coherences results in the observation of cross peaks at frequencies $(\nu_{1,\alpha} + \nu_{1,\beta}, \nu_{1,\beta} + \nu_{1,\alpha})$. Moreover, cross peaks due to single-quantum−double-quantum combinations are also observed. The different combination peaks are evidenced in the simulations of Figure 3. The single-quantum ridges due to the two interacting protons are in red and cyan and overlap almost completely, in particular at the parallel position. In magenta, combinations of the types $(\nu_{1,\alpha}, \nu_{1,\beta} + \nu_{2,\beta})$ and $(\nu_{2,\alpha}, \nu_{1,\beta} + \nu_{2,\beta})$ are evidenced, while combinations of the types $(\nu_{1,\beta}, \nu_{1,\alpha} + \nu_{2,\alpha})$ and $(\nu_{2,\beta}, \nu_{1,\alpha} + \nu_{2,\alpha})$ are in green. The ridges due to correlation of DQ coherences are in black. These DQ ridges are particularly informative, as they allow determination of the relative sign and orientation of the hyperfine tensors.[16] We simulated the shape of the combination-frequency ridges assuming different couplings and orientations of the contributing protons (see Supporting Information). The simulation analysis indicates that the shape and extension of the DQ ridges can be reproduced assuming two interacting protons with slightly different couplings and with $|A_{1\parallel}|, |A_{2\parallel}| > |A_{1\perp}|, |A_{2\perp}|$. The extension of the DQ ridges at the two magnetic field settings corresponding to $g = g_\parallel$ and $g = g_\perp$ also indicates that the two tensors are noncoaxial with respect to the g_{zz} (C_3) axis, forming angles of 70° and 50°, respectively. The ^{1}H hyperfine tensors extracted from the simulation analysis are reported in Table 1.

The parameters obtained from the simulation of the SMART HYSCORE spectra have been used to simulate the standard HYSCORE spectra of Figure 2 and the ^{1}H Davies ENDOR spectra (see Supporting Information Figures S2 and S3).

The simulation analysis unambiguously shows that the three tensor elements of the ^{1}H coupling matrix must have the same sign. Assuming the sign of T as positive (g_n for H is positive) and representing the principal values of the dipolar tensor as $[-T\ -T\ 2T]$, with T defined as

$$T = \frac{\mu_0}{4\pi} g_e g_n \beta_e \beta_n \frac{1}{r^3} \qquad (1)$$

dx.doi.org/10.1021/ic1021802 |Inorg. Chem. 2011, 50, 2385–2394

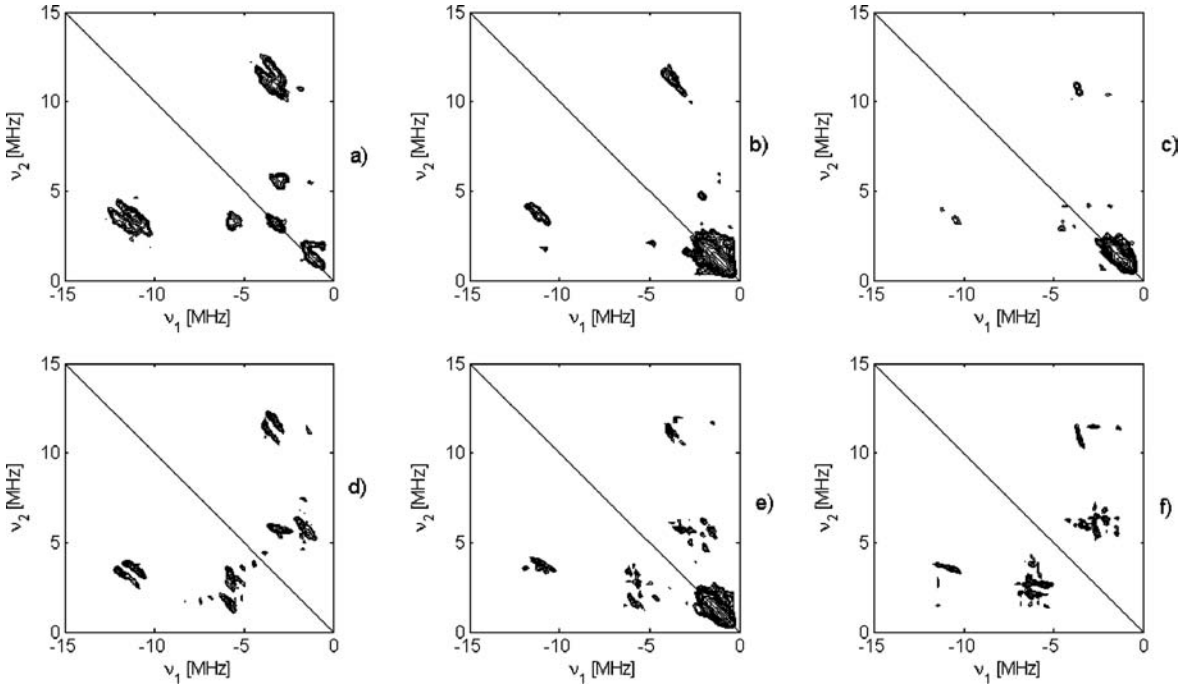

Figure 4. (a) ^{17}O HYSCORE spectra taken at observer positions: (a) B_0 = 366.0 mT (position 3 in Figure 1a), (b) B_0 = 352.0 mT (position 2 in Figure 1a), and (c) B_0 = 349.0 mT (position 1 in Figure 1a). The corresponding computer simulations are reported in parts d, e, and f. Spectra were recorded with τ = 144 ns at 10 K.

the values of a_{iso} = 7.5 MHz and T = 4.0 MHz and a_{iso} = 4.8 MHz and T = 3.3 MHz were obtained for the two sets of protons, in agreement with DFT calculations (vide infra).

Assuming the anisotropic part of the hyperfine interaction to be described as a purely point-dipolar interaction, the distance between the proton and the metal cation can be estimated from eq 1 to be about 0.27 and 0.29 nm for protons 1 and 2, respectively.

Note that the above approach is an approximation, but since the spin density on the ^{17}O nuclei is small (<0.2%, see further), it can be used to obtain a good first indication of the proton−Ti distance.

The a_{iso} of water protons coordinated to transition-metal ions is very sensitive to the orientation of the water molecule with respect to the plane containing the unpaired electron. For the case of $VO(H_2O)_5^{2+}$ species, DFT calculations[35] have shown that the proton hyperfine coupling constant is sensitive to orientation and varies from +10 to −1 MHz as a function of rotation of the H−O−H plane with respect to the plane where the orbital containing the unpaired electron dwells. In particular, positive proton hyperfine couplings with a relatively large magnitude (∼10 MHz) are indicative of water molecules oriented in or nearly in the plane containing the unpaired electron. On the contrary, negative proton hyperfine coupling constants that are small in magnitude are associated with water molecules oriented perpendicular to that plane.

In our case, assuming the D_{3d} symmetry of the complex, the maximum spin density is along the C_3 axis (see Figure 6). It is then conceivable that the overlap between the orbital hosting the unpaired electron (d_{z^2}) and the water molecular orbitals will be maximized when the hydrogens are oriented along the C_3 axis (D_{3d} "all vertical") and minimized when the H−O−H plane is perpendicular to the same axis (D_{3d} "all horizontal").[34]

^{17}O HYSCORE and Davies-ENDOR Spectra. In order to thoroughly characterize the local environment of the Ti^{3+} esaquo species, HYSCORE experiments have been performed on a ^{17}O-enriched sample. The HYSCORE spectra recorded at different magnetic fields are reported in Figure 4 together with the corresponding computer simulation. None of the ^{17}O HYSCORE spectra exhibit combination-frequency cross peaks, because of the low average number of ^{17}O nuclei per complex combined with the intrinsic lower intensity of these cross peaks.

The spectra recorded at the observer position $g = g_\perp$ (Figure 4a) are dominated by the presence of cross peaks in the ∓ quadrant at approximately (−11, 3.5) MHz and (−3.5, 11) MHz, which are absent in the sample with $H_2{}^{16}O$ and can be ascribed to DQ transitions arising from the hyperfine interaction of the unpaired electron with a ^{17}O nucleus (I = 5/2). The cross peaks at ∼(−2,5) MHz and (−5,2) MHz relate the m_I 1/2 → −1/2 transitions of the two m_S manifolds. These transitions are the least affected by the nuclear quadrupole interaction, and their frequencies are given to first order (neglecting the quadrupole interaction) by $\nu_{\alpha(\beta)} = (A/2 \pm \nu_I)$, where A represents the hyperfine coupling for the given orientation of the paramagnetic species and ν the ^{17}O Larmor frequency. The values of A estimated from the HYSCORE spectra recorded at observer positions corresponding to $g = g_\perp$ (366 mT) and $g = g_\parallel$ (352 mT) are respectively ∼6.6 MHz and ∼8.5 MHz. These values agree with Davies-ENDOR spectra taken at the same observer positions, which are shown in Figure 5 along with their simulation.

At the two observer positions, the ^{17}O peaks are approximately centered at half the hyperfine coupling, (∼3.5 MHz at B_0 = 366.0 mT and ∼4 MHz at B_0 = 352.0 mT), split by twice the nuclear Zeeman frequency (∼2.0 MHz × 2), and split by the nuclear quadrupole coupling. This latter splitting is actually unresolved in the experimental spectrum and contributes to the broadening of the spectral line width.

dx.doi.org/10.1021/ic1021802 |Inorg. Chem. 2011, 50, 2385–2394

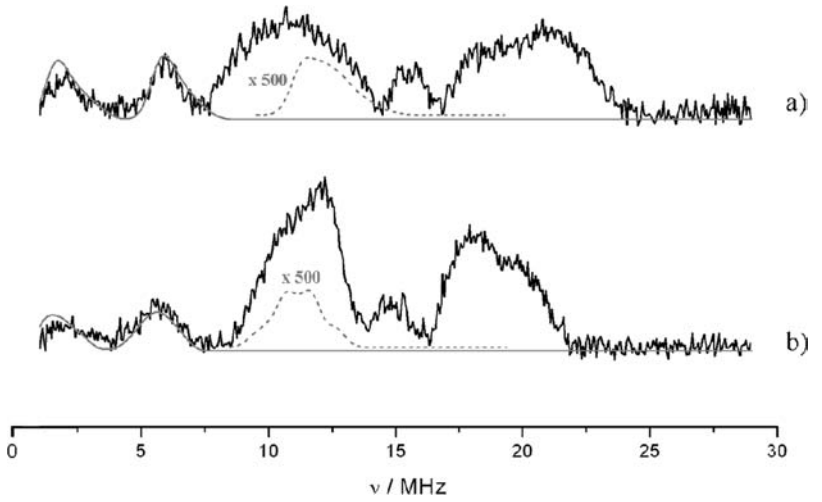

Figure 5. Davies-ENDOR spectra of $[Ti(H_2{}^{17}O)_6]^{3+}$ measured at 4 K at (a) B_0 = 366.0 mT and (b) B_0 = 352.0 mT. At each position, the black line is the experimental data, and the gray is the simulation. Only the spectral contributions due to the interactions with the ^{17}O nuclei are simulated. The dotted line is a magnification of the simulated spectra in the region of the ^{17}O double-quantum transitions.

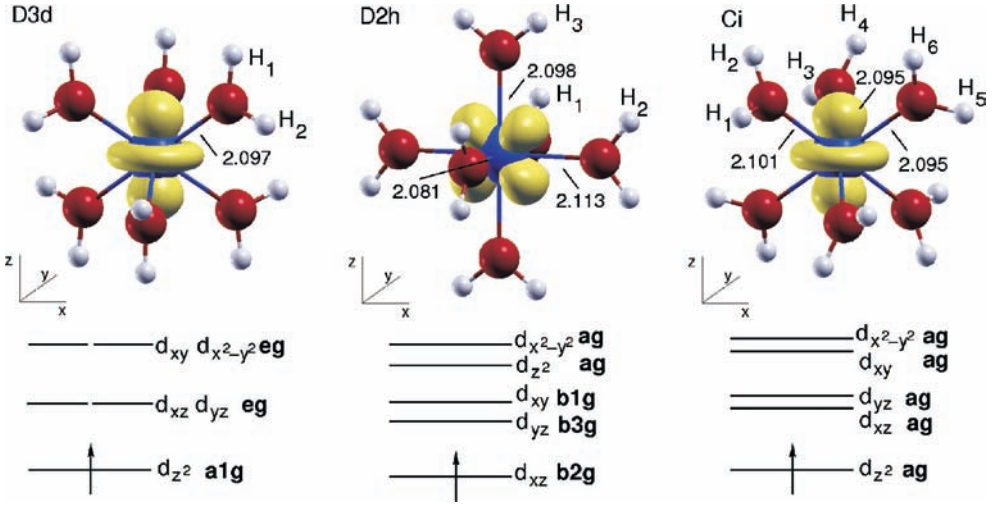

Figure 6. Upper panel: Ball and stick representation of the $[Ti(H_2O)_6]^{3+}$ complex in the three point symmetries considered. Magnetically nonequivalent protons reported in Table 2 are labeled. The *z*-axis of the coordinate frame shown next to each complex corresponds to the principal *z*-axis of the ***g***-tensor, as assigned in Table 2. Lower panel: d-orbital occupation, symmetry and energy order for the Ti ion in the three coordination spheres.

The estimated hyperfine values have been used as starting values for the simulations of both HYSCORE and ENDOR spectra reported in Figures 4 and 5. The simulation analysis of the HYSCORE spectra was carried out considering the effect of a_{iso} and nuclear quadrupole interaction on the spectral pattern (see the Supporting Information). Given the high number of parameters, which concur to determine the HYSCORE spectrum of ^{17}O, we used the Euler angles extracted from DFT computations (*vide infra*) and searched for the eigenvalues of the hyperfine and quadrupole tensors. The tensor orientations obtained from DFT and adopted in the simulation are reported in the Supporting Information. The DFT results gave different Euler angles of the **A** and **Q** tensors for the different water ligands reflecting the symmetry of the complex. According to the DFT results, we based our simulation on the D_{3d} symmetry (see Figure 6, Table 1). The simulations reported in Figure 4 were thus obtained by adding together the simulation obtained for each of the six individual oxygen nuclei. Summation of the individual contributions is valid in this case, since almost half of the labeled complexes have only one ^{17}O nucleus (see the Sample Preparation section). The intensities of the simulated spectra were then scaled to fit the experimental results. The simulation analysis shows that the main features of the spectra recorded at different field positions can be well reproduced with the following tensor **A** = [7 9.5 6] MHz, where the smallest hyperfine component is directed along the Ti−O bond tilted by 64° with respect to the g_z direction, while the largest hyperfine components point in a direction perpendicular to the plane of the water molecule (see Figure S4 in the Supporting Information).

These same values provide a good fit of the Davies ENDOR spectra. We notice that at approximately 11.5 MHz the double quantum transition observed in the HYSCORE spectrum is also predicted by the ENDOR simulation, albeit with low intensity (see dotted lines in Figure 5). Indeed, the increased intensity in the low-frequency region of the proton ENDOR spectrum, observed when ^{17}O-labeling is used, matches the region where

dx.doi.org/10.1021/ic1021802 |*Inorg. Chem.* 2011, 50, 2385–2394

the double-quantum transitions are expected (^{17}O and ^{16}O Davies-ENDOR difference spectra are presented as Supporting Information Figure S7). It should be noted that although the ENDOR spectra reported in Figure S7 of the Supporting Information, were taken under the same experimental conditions, the replacement of the ^{16}O by ^{17}O can have an influence on the relaxation rates of the other nuclei, which will influence the spectral line intensities. This, together with the fact that simulations do not take into account the microwave pulse lengths, explains why the ^{17}O double-quantum peak predicted by the simulations in Figure 5 is 500 times weaker than the single quantum lines, despite the fact that in the ^{17}O−^{16}O spectral subtraction (Figure S7) these have the same intensity.

The hyperfine tensor can be decomposed into the Fermi contact and dipolar components, leading to a_{iso} = 7.5 MHz and $T = [-0.5 \pm 0.5; +2.0 \pm 0.5; -1.5 \pm 0.5]$ MHz, where the sign of a_{iso} has been taken as positive as determined from NMR measurements of the Ti(III) aquo complex.[36]

The a_{iso} value extracted from our data is significantly larger than the value reported from NMR studies of about 4 MHz. Its positive value can be rationalized considering a spin polarization mechanism to be dominant, which suggests an important role of π bonding in the ion−ligand bonding. The a_{iso} term (Fermi contact term) arises from the finite probability of finding an unpaired electron spin on an atomic s orbital. By a direct mechanism, a fraction of an electronic spin is delocalized to an s orbital, and as a result a positive a_{iso} value is observed for the ^{1}H nuclei (negative for the ^{17}O nuclei with g_n negative). On the other hand, unpaired electron spin density in a p orbital effectively polarizes the electrons in the s, orbital inducing a negative spin. This spin-polarization mechanism leads to a negative proton (or positive ^{17}O) hyperfine coupling. The positive oxygen-17 a_{iso} term can be anticipated considering the relevant molecular orbitals involved in the bonding. In the water molecule, the highest occupied orbital ($1b_1$) is nonbonding and highly localized on the oxygen atom, with prevalent p_z character and π symmetry. The next lowest orbital ($2a_1$) has σ symmetry and results from the combination of oxygen $2p_z$ and hydrogen 1s orbitals. It can be thought of as a nonbonding orbital, as it has a lobe pointing away from the two hydrogens. At lower energy, another π symmetry orbital ($1b_2$) is found as a result of the combination of oxygen $2p_y$ and hydrogen 1s orbitals. Being the unpaired electron in a t_{2g} orbital (b_2), a π bonding is to be expected, leading to the observed spin polarization at the oxygen nucleus. In the same way, a π mechanism will place directly unpaired spin at the hydrogen nucleus, thus explaining the large and positive Fermi contact term experimentally observed. Consistent with this frame are the ^{17}O a_{iso} values reported in the literature for other transition-metal ion aquo complexes. Fermi contact terms of similar magnitude and sign to those observed in this work have been observed for vanadyl(IV) aquo complexes, which also have a single unpaired electron in a b_2-type orbital.[9] On the contrary, large values, opposite in sign to those found for the d^1 complexes, have been found for hydrated Cu^{2+} [37] and Ni^{2+},[38] in which the unpaired electrons are confined in e_g orbitals and σ bonding mechanisms are dominant.

From the 17-oxygen dipolar term, the Ti−O distance can be estimated making use of eq 1. Considering that the hyperfine coupling is dominated by the Fermi contact term, eq 1 can only give an indicative value of 0.20 ± 0.03 nm, which is in accordance with values reported in the literature[6] and compatible with the results of DFT modeling (vide infra).

The splitting of the DQ transitions arises from the nuclear quadrupole interaction and is found to be sensitive to the asymmetry parameter η. From the simulation, the following nuclear quadrupole coupling parameters are extracted $|e^2qQ/h|$ = 6.0 ± 0.5 MHz and η = 0.5 ± 0.1. The 17-oxygen e^2qQ/h is in line with the typical values reported for water in ice[39] (6.5 MHz) and in frozen solutions of other transition metal esaquo complexes, where values ranging between 7 and 6 MHz have been reported.[9,10,40]

Analysis of the ^{1}H HYSCORE spectra points to a situation where the water protons are oriented along the C_3 symmetry axis and lie in the same plane. This requires that the Ti(III) ions reside in the H−O−H plane, with the bisector of the lone pairs of the water oxygen oriented toward the ion. This situation has been considered by Sikka et al.[41,42] and more recently in the case of water coordination to Gd^{3+} ions.[10]

Theoretical Calculations. Three point-group symmetries have been investigated, D_{3d}, D_{2h}, and C_i, as possible minimum energy structures of the potential energy surface of the $[Ti(H_2O)_6]^{3+}$ complex. The three structural isomers are close in energy, being separated by at most 0.2 eV. As reported by Kallies and Meier,[34] based on B3LYP calculations, we also found that C_i is the most stable structure, separated by 70 meV from the D_{3d} isomer and by 230 meV from the least stable D_{2h} structure. The Ti−O bond lengths and the energy order of the Ti d orbitals are reported in Figure 6 in order of decreasing symmetry.

In the highly symmetric D_{3d} complex, all Ti−O bonds have the same length (2.097 Å), and the unpaired electron is hosted in a d_{z^2} orbital (a_{1g}). The unoccupied d states form two pairs of degenerate states (e_g).

The D_{2h} symmetry is characterized by three pairs of equivalent bonds. Each pair lies on the direction of a C_2 axis of the system. The unpaired electron is in a d_{xz} (b_{2g}) orbital, and there is no degeneracy for the empty d states.

The structural configuration of the C_i symmetry is essentially very similar to that of the D_{3d}, but the OH bonds are all rotated from the in plane D_{3d} position by about 20°. This is the reason for the disappearance of many symmetry operations. The unpaired electron is hosted in a d_{z^2} orbital (a_g), and there is no degeneracy for the remaining unoccupied d orbitals. However, the energy differences within the pairs $d_{yz} - d_{xz}$ and $d_{xy} - d_{x^2-y^2}$ are even smaller than in the case of the D_{2h} symmetry.

For each point symmetry, the EPR parameters (**g** tensor and hyperfine coupling constants) and electronic transitions were computed. In the case of the D_{3d} symmetry, some methodological tests have been performed. In particular, we considered (i) the effect of the amount of exact exchange in the exchange-correlation functional and (ii) the effect of the solvent. The amount of exact exchange may have an effect on the degree of localization of the unpaired electron on the central cation and, consequently, on the values of the hyperfine coupling constants of the ligands. We have compared density functionals which contain from 0% to 30% of exact exchange (0% (BLYP), 13% (HF(13)-LYP), 20% (B3LYP), 30% (HF(30)-LYP)). The results, however, show very small changes in the hyperfine coupling constants with the method used. Also, the solvating effect of water, described with a polarizable continuum model (PCM), is found to be negligible (Table 2). However, it should be mentioned that the explicit interaction of the water ligands through hydrogen bonding with water ligands from other complexes or from the solvent has not been considered. The theoretical model is that of an isolated $[Ti(H_2O)_6]^{3+}$ complex. Discrepancy

Table 2. Relative Stability (in eV), Optical Excitations (in nm), and Experimental Spin Hamiltonian Parameters (in MHz) for the Hydrated Ti^{3+} Ion

						^{1}H					^{17}O							
	ΔE (eV)	T_e (nm)	$g_\parallel$		$g_\perp$	a_{iso}	T_x	T_y	T_z	β [a]	a_{iso}	T_x	T_y	T_z	β [a]	e^2qQ/h	η	β [a]
exp.		505	1.994		1.896	4.8 ± 0.2	−3.3 ± 0.2	−3.3 ± 0.2	+6.6 ± 0.2	50 ± 5	7.5 ± 0.5	−0.5 ± 0.5	+2.0 ± 0.5	−1.5 ± 0.5	64	6.0 ± 0.5	0.5 ± 0.1	31
		570				7.5 ± 0.2	−4.0 ± 0.2	−4.0 ± 0.2	+8.0 ± 0.2	70 ± 5								
D_{3d}																		
B3LYP	+0.07	514	2.000		1.884	6.6	−3.7	−3.6	7.3	45	6.7	−0.5	1.7	−1.2	64	9.8	0.53	31
						7.7	−3.5	−3.4	7.0	72								
B3LYP + solvent effect			2.000		1.893	8.1	−3.9	−3.9	7.8		6.9	−0.4	1.7	−1.2				
						9.4	−3.6	−3.5	7.1									
HF-13			2.000		1.888	7.1	−3.6	−3.6	7.3		7.0	−0.6	1.9	−1.2				
						8.3	−3.5	−3.4	6.9									
HF-30			2.000		1.877	6.1	−3.7	−3.6	7.3		6.3	−0.4	1.6	−1.2				
						7.0	−3.5	−3.5	7.0									
BLYP			1.999		1.905	7.4	−3.6	−3.5	7.1		6.2	−0.8	2.2	−1.4				
						9.0	−3.4	−3.3	6.7									
D_{2h}			g_z	g_x	g_y													
B3LYP	+0.23	499	1.890	1.932	1.924	−0.4	−3.5	−2.9	6.4	78[b]	5.0	−0.2	1.3	−1.1	0	10.1	0.51	0
						10.8	−3.8	−3.7	7.5	75	7.6	−0.6	1.7	−1.1	90	10.3	0.50	90
		508				11.6	−3.8	−3.7	7.5	15[b]	7.8	−0.7	2.1	−1.4	90	9.6	0.54	90
C_i			g_z	g_x	g_y													
B3LYP	0.0	559	2.000	1.848	1.840	4.4	−3.7	−3.2	6.9	73[b]								
						3.9	−3.9	−3.5	7.4	45[b]	5.4	−0.2	1.5	−1.3	86	9.7	0.53	34
						5.0	−3.9	−3.5	7.4	76	5.9	−0.5	1.4	−1.0	64	9.6	0.54	37
		565				5.4	−3.7	−3.3	7.0	72	5.5	−0.4	1.3	−1.0	28	9.7	0.54	41
						3.7	−3.9	−3.4	7.3	45								
						4.1	−3.6	−3.2	6.8	68								

[a] See the Supporting Information for the definition of the orientations, β is in degrees. [b] The smaller angle between the **g** and **T** tensors' z-axis directions is reported.

dx.doi.org/10.1021/ic1021802 |*Inorg. Chem.* 2011, 50, 2385–2394

between the experimental and computed nuclear quadrupole coupling constant for ^{17}O could originate from this approximation, as will be discussed in the next section. For the D_{3d} complex, the **g** tensor is purely axial, while the **A** tensors for the O and the H nuclei are slightly distorted from the axial symmetry.

The EPR parameters computed for the D_{2h} symmetry present clear differences with respect to those for the D_{3d} symmetry. The **g** tensor is characterized by a very low g component ($g_z = 1.890$), largely shifted from the free electron value, and two very close components ($g_x = 1.932$ and $g_y = 1.924$). The structure of the **g** tensor is thus completely different from that observed experimentally. Furthermore, the DFT calculations indicate this as the least stable structure. Thus, both energy considerations and the symmetry of the complex allow us to rule this out as the structure of the complex.

In the case of C_i point symmetry, the **g** tensor is almost axial, Table 2, and the difference in the g_x and g_y components could be difficult to appreciate experimentally. Six nonequivalent protons and three nonequivalent oxygens atoms are identified on the basis of the hyperfine coupling constants, although differences among them are very small, certainly below the detection limit. Note that the oxygen orientations remain unaltered with respect to the D_{3d} case.

Electronic transitions in the visible region have been computed by means of the TD-DFT approach. In the case of D_{3d} point symmetry, two degenerate transitions ($d_{z^2} \rightarrow d_{xy}$ and $d_{z^2} \rightarrow d_{x^2-y^2}$) at 514 nm are found. For the D_{2h} point symmetry, two transitions are computed at similar wavelengths, 499 and 508 nm ($d_{xz} \rightarrow d_{z^2}$ and $d_{xz} \rightarrow d_{x^2-y^2}$). Also, in the case of C_i, there are two nondegenerate transitions at slightly higher wavelengths, 559 and 565 nm ($d_{z^2} \rightarrow d_{xy}$ and $d_{z^2} \rightarrow d_{x^2-y^2}$). All of the computed transitions are thus in quite good agreement with the experiment, which shows a broad absorption band in the region around 500 nm. The two excited state transitions found in D_{2h} and C_i, however, are separated by little energy, which reflects the near degeneracy of the corresponding orbitals involved in the transition. In this respect, it should be mentioned that the origin of the second band in the experimental spectrum, separated by about 70 nm from the main absorption line, is not related to the breaking of degeneracy following distortion to D_{2h} or in C_i complexes, but rather to the dynamic or excited Jahn−Teller effect. A proper treatment of this transition may require more sophisticated theoretical approaches and goes beyond the scopes of this work.

DISCUSSION AND CONCLUSIONS

The results from the CW and pulse EPR and ENDOR experiments provide a very detailed description of the electronic structure of the $[Ti(H_2O)_6]^{3+}$ complex. The data can be interpreted as due to a distortion of the complex from octahedral O_h symmetry to D_{3d}. This is indeed the current interpretation which can be found in textbooks. The comparison with *ab initio* electronic structure calculations reinforces this view. Not only is the axial structure of the **g** and the **A** tensor reproduced but there is a quantitative agreement for both observable quantities, Table 2. This is true not only for the hyperfine coupling constants of the unpaired electron on Ti with the ^{17}O atoms of the water ligands but also for the superhyperfine interactions with the protons. There are some minor deviations in terms of the isotropic component, on the order of 1 or 2 MHz, but it is known that this quantity is hard to reproduce quantitatively due to the need to describe with great accuracy the Fermi contact term, which in turn depends on the description of the core orbitals of the system. Also, the angle β between the z components of the **g** and the **T** tensors is reproduced quantitatively for both O and H nuclei, Table 2. The only discrepancy is related to the nuclear quadrupole interaction, which in the calculations is about two times larger than in the experiment. This discrepancy can, however, be explained taking into account the hydrogen bonding interactions present in the real system and neglected in the calculations. Hydrogen bonding effectively decreases the difference in the electron populations between the O lone pairs and the electronic population in the OH bond, thus altering the electric field gradient at the nucleus and hence the nuclear quadruple tensor. Indeed, the major quadrupole interaction in H_2O decreases with the strength of hydrogen bonding going from about 10 MHz in the gas phase[43] (in agreement with computations) to about 6 MHz in ice[39,44] (in line with the value found in the experiment). Values ranging from 6 to 7 MHz have been reported for ^{17}O nuclear quadrupole interactions of different transition-metal-ion aquo complexes.[9,40] The same trend between experimental and calculated ^{17}O nuclear quadrupole couplings is observed in ref 9 in the case of the $[Mn(H_2O)_6]^{2+}$ complex.

These data essentially reinforce the current assignment of the structure of the $[Ti(H_2O)_6]^{3+}$ complex to a D_{3d} symmetry. However, as mentioned in the previous section and as first reported by Kallies and Meier,[34] this is *not* the ground state of the system. There is a small but clear energy difference in favor of the low symmetry C_i complex, which can be obtained from the D_{3d} case by small rotations of the water ligands. The computed EPR properties for this lower symmetry case are also quite consistent with the experimental spectrum. The **g** tensor is no longer axial, but the difference between the g_x and g_y components is below the instrumental resolution. The three nonequivalent O atoms and the six nonequivalent H atoms exhibit average a_{iso} and T values which are virtually indistinguishable from those of the D_{3d} complex. Also, the average Euler angles are essentially the same. In summary, the theoretical observable properties of the $[Ti(H_2O)_6]^{3+}$ complex are consistent with the experiment for both D_{3d} and C_i complexes (but not for the D_{2h} one), while energy arguments are in favor of the C_i structure.

On this basis, we conclude that the $[Ti(H_2O)_6]^{3+}$ complex has two structural isomers which are very close in energy, D_{3d} and C_i, and both consistent with a very accurate experimental characterization. For the isolated (gas-phase) complex, the C_i isomer is slightly favored in energy. However, due to the fact that H bonding was not taken into account in the calculations and considering that thermally averaged parameters are likely to be measured in the experiment, a firm conclusion on the nature of the ground state of $[Ti(H_2O)_6]^{3+}$ complexes cannot be made. It is clear however that the C_i complex should be considered in future discussions on the nature of this system.

Moreover, this study demonstrates that HYSCORE spectroscopy in conjunction with DFT calculations has enormous potential in gaining structural information on Ti(III) systems. Indeed, this approach, which involves 17-O labeling, seems to be promising in the study of more sophisticated systems such as chelate complexes of interest in homogeneous catalysis or Ti-based solid-state systems, which found applications in a vast range of scientific and technological areas.

ASSOCIATED CONTENT

Supporting Information. Simulation analysis of the ^1H SMART HYSCORE spectra. Experimental and simulated ^1H

dx.doi.org/10.1021/ic1021802 |*Inorg. Chem.* 2011, 50, 2385–2394

HYSCORE and ^{1}H Davies ENDOR spectra taken at different field positions. Schematic illustration of the ^{17}O hyperfine and quadrupole tensor orientations. Simulation analysis of the ^{17}O HYSCORE spectra. ^{17}O and ^{16}O Davies ENDOR difference spectra. This material is available free of charge via the Internet at http://pubs.acs.org.

AUTHOR INFORMATION

Corresponding Author

*E-mail: m.chiesa@unito.it.

REFERENCES

(1) Arrhenius, S. A. *Z. Phys. Chem.* **1887**, *1*, 631.
(2) Ohtaki, H.; Radnai, T. *Chem. Rev.* **1993**, *93*, 1157.
(3) Corma, A.; Garcia, H. *Chem. Rev.* **2002**, *102*, 3837.
(4) (a) Gourier, D.; Samuel, E. *J. Am. Chem. Soc.* **1987**, *109*, 4571. (b) Horáček, M.; Kupfer, V.; Thewalt, U.; Polašek, M.; Mach, K. *J. Organomet. Chem.* **1999**, *579*, 126. (c) Prakash, A. M.; Kevan, L.; Zahedi-Niaki, M. H.; Kaliaguine, S. *J. Phys. Chem. B* **1999**, *103*, 831. (d) Aono, M.; Hasiguti, R. R. *Phys. Rev. B* **1993**, *48*, 12406. (e) Howe, R. F.; Grätzel, M. *J. Phys. Chem.* **1985**, *89*, 4495. (f) Van Doorslaer, S.; Shane, J. J.; Stoll, S.; Schweiger, A.; Kranenburg, M.; Meier, R. J. *J. Organomet. Chem.* **2001**, *634*, 185.
(5) Cotton, F. A.; Wilkinson, G. *Advanced Inorganic Chemistry*; John Wiley and Sons: New York, 1988.
(6) Tachikawa, H.; Ichikawa, T.; Yoshida, H. *J. Am. Chem. Soc.* **1990**, *112*, 977.
(7) Tachikawa, H.; Ichikawa, T.; Yoshida, H. *J. Am. Chem. Soc.* **1990**, *112*, 982.
(8) Schweiger, A.; Jesche, G. *Principles of Pulse Electron Paramagnetic Resonance*; Oxford University Press: Oxford, U. K., 2001.
(9) Baute, D.; Goldfarb, D. *J. Phys. Chem. A* **2005**, *109*, 7865.
(10) Raitsimring, A. M.; Astashkin, V.; Baute, D.; Goldfarb, D.; Caravan, P. *J. Phys. Chem. A* **2004**, *108*, 7318.
(11) Astashkin, A. V.; Johnson-Winters, K.; Klein, E. L.; Feng, C.; Wilson, H. L.; Rajagopalan, K. V.; Raitsimring, A. M.; Enemark, J. H. *J. Am. Chem. Soc.* **2008**, *130*, 8471.
(12) Su, J. H.; Lubitz, W.; Messinger, J. *J. Am. Chem. Soc.* **2008**, *130*, 786.
(13) Chiesa, M.; Giamello, E.; Di Valentin, C.; Pacchioni, G.; Sojka, Z.; Van Doorslaer, S. *J. Am. Chem. Soc.* **2005**, *127*, 16935.
(14) Stoll, S.; Schweiger, A. *J. Magn. Reson.* **2006**, 42–55.
(15) Höfer, P.; Grupp, A.; Nebenführ, H.; Mehring, M. *Chem. Phys. Lett.* **1986**, *132*, 279.
(16) Liesum, L.; Schweiger, A. *J. Chem. Phys.* **2001**, *114*, 9478.
(17) Jeschke, G.; Rakhmatullin, R.; Schweiger, A. *J. Magn. Reson.* **1998**, *131*, 261.
(18) Madi, Z. L.; Van Doorslaer, S.; Schweiger, A. *J. Magn. Reson.* **2002**, *154*, 181.
(19) Frisch, M. J. et al. *Gaussian 03*, Revision A.7; Gaussian Inc.: Pittsburgh, PA, 2003.
(20) Hay, P. J.; Wadt, W. R. *J. Chem. Phys.* **1985**, *82*, 299.
(21) Krishnan, R.; Binkley, J.; Seeger, R.; Pople, J. *J. Chem. Phys.* **1980**, *72*, 650.
(22) Barone, V. In *Recent Advances in Density Functional Methods Part I*; Chong, P. I., Ed.; World Scientific Publ. Co.: Singapore, 1996.
(23) Becke, A. D. *Phys. Rev. A* **1988**, *38*, 3098.
(24) Lee, C.; Yang, W.; Parr, R. G. *Phys. Rev. B* **1998**, *37*, 785.
(25) Becke, A. D. *J. Chem. Phys.* **1993**, *98*, 5548.
(26) Miertuš, S; Tomasi, J. *Chem. Phys.* **1982**, *65*, 239.
(27) Furche, F.; Ahlrich, R. *J. Chem. Phys.* **2002**, *117*, 7433.
(28) Neese, F. *J. Chem. Phys.* **2001**, *115*, 11080.
(29) Wilson, R. C.; Mayers, R. J. *J. Chem. Phys.* **1976**, *64*, 2208.
(30) Premović, P. I.; West, P. R. *Can. J. Chem.* **1975**, *53*, 1630.
(31) Wang, F.; Xiao-Xuan, W.; Wen-Chen, Z. *J. Phys. Chem. Solids* **2007**, *68*, 131.
(32) McGarvey, B. R. *J. Chem. Phys.* **1963**, *38*, 388.
(33) Hartmann, M.; Clark, T.; van Eldik, R. *J. Phys. Chem. A* **1999**, *103*, 9899.
(34) Kallies, B.; Meier, R. *Inorg. Chem.* **2001**, *40*, 3101.
(35) Saladino, A. C.; Larsen, S. C. *Catal. Today* **2005**, *105*, 122.
(36) Reuben, J.; Fiat, D. *Inorg. Chem.* **1969**, *8*, 1821.
(37) Lewis, W. B.; Alei, M.; Morgan, L. O. *J. Chem. Phys.* **1966**, *44*, 4103.
(38) Connick, R. E.; Fiat, D. *J. Chem. Phys.* **1966**, *44*, 2409.
(39) Edmonds, D. T.; Zussman, A. *Phys. Lett. A* **1972**, *41*, 167.
(40) Tan, X.; Bernardo, M.; Thomann, H.; Scholes, C. P. *J. Chem. Phys.* **1995**, *117*, 8243.
(41) Chidambaram, R.; Sequeira, A.; Sikka, S. K. *J. Chem. Phys.* **1964**, *41*, 3616.
(42) Sikka, S. K.; Momin, S. N.; Rajagopal, H.; Chidambaram, R. *J. Chem. Phys.* **1968**, *48*, 1883.
(43) Verhoeven, J.; Dymanus, A.; Bluyssen, H. *J. Chem. Phys.* **1969**, *50*, 3330.
(44) Spiess, H. W.; Garrett, B. B.; Sheline, R. K.; Rabideau, S. W. *J. Chem. Phys.* **1969**, *51*, 1201.